Article

Femtosecond Pulsed Laser Irradiation of Zirconia for Embedding Silver Nanoparticles in Surface Nanopores

Yuka Yamamuro [1] , Tomotaka Shimoyama [2], Hiroya Nagata [2] and Jiwang Yan [1],*

[1] Department of Mechanical Engineering, Faculty of Science and Technology, Keio University, Hiyoshi 3-14-1, Kohoku-ku, Yokohama 223-8522, Japan; y.yamamuro@keio.jp
[2] Inorganic Materials Research Laboratory, Tosoh Corporation, Hayakawa 2743-1, Ayase 252-1123, Japan; tomotaka-shimoyama-xq@tosoh.co.jp (T.S.); hiroya-nagata-yg@tosoh.co.jp (H.N.)
* Correspondence: yan@mech.keio.ac.jp; Tel.: +81-45-566-1445

Featured Application: Functional surfaces of zirconia with antibacterial properties.

Abstract: Femtosecond pulsed laser irradiation was performed to investigate the feasibility and fundamental characteristics of embedding silver nanoparticles onto zirconia ceramic surfaces. By irradiating laser, nanopores were fabricated on the surface of the yttria-stabilized zirconia (YSZ) substrate, and silver nanoparticles were infiltrated and immobilized into the pores using a commercial nano-silver dispersion solution. Numerous nanopores embedded with silver nanoparticles were successfully obtained on the YSZ surface while keeping the grains' shapes unchanged by controlling laser parameters. Optimizing laser fluence and scanning speed near the ablation threshold made it possible to remove only the excess dispersant that remained on the surface while keeping silver in the pores and without causing machining of the surface of the YSZ substrate. In addition, about 60% embedding in the nanopores was achieved. It was found that the shorter pulse width was suitable to avoid evaporating both dispersant and silver. Cross-sectional observation revealed that the silver nanoparticles were agglomerated to form clumps and were embedded without a gap at the bottom of the pores at a depth of about 600 nm. After laser irradiation, no significant laser-induced phase change was observed in the YSZ substrate, indicating that there was no in-process thermal damage to the bulk. These findings demonstrated the possibility of adding a metal nanoparticle to the zirconia surface by using only a laser process without damaging the properties of the base material during the process. New applications of zirconia, such as the generation of functional surfaces with antibacterial properties, are expected.

Keywords: nanopore; yttria-stabilized zirconia; femtosecond pulsed laser; silver; phase transformation; ceramic material

1. Introduction

Zirconia (ZrO$_2$) is an important ceramic material with excellent heat resistance, hardness, chemical stability, and unique aesthetic effects. In particular, polycrystalline tetragonal yttria-stabilized zirconia (YSZ) shows high strength and high fracture toughness at room temperature thanks to the effect of the stress-induced phase transformation mechanism [1]. Due to its superior properties, YSZ has been used in many applications such as dental implants, biomaterial components, and mechanical components, and has increasing demand in various fields. To improve the functionality of these YSZ products and to develop new applications, there is a need for higher surface functionality.

For the surface functionalization, there are various approaches. Surface micro/nanoscale structures can change and enhance many surface functionalities such as wettability [2], anti-fouling [3], biocompatibility [4,5], and frictional properties [6]. It is also effective to immobilize various materials on the surface that are different from the base material. By loading various materials, such as metal nanoparticles, new functions can be obtained, such

as antimicrobial and optical properties, which are limited in expression by treatment of the base material alone. For example, by selecting metal nanoparticles into silver and attaching them to graphene oxide [7] or cellulose nanofibers [8], it is possible to create new materials with antibacterial properties [9]. Surface treatment methods include coating, plating, and glazing, which cover the entire surface. However, depending on the application, these methods may change the surface topography by adding a new layer on the substrate or may change the surface functionality and appearance of the substrate itself by covering the substrate. Therefore, in order to take advantage of the surface characteristics of the substrate itself, it is effective to use a method in which the desired material is loaded locally only on a part of the substrate. For example, if a nanostructure is created on the surface and the desired materials are placed in it, it is expected that the materials can be fixed in the structure without covering the entire substrate surface. Zachman et al. [10] proposed the nanopore delivery system, in which nanopore arrays are made on fused silica substrates, effectively loading peptides by adsorption.

However, although zirconia is excellent as a support due to its chemical stability, it is difficult to process nanostructures on the zirconia surface. Lithography [3] and anodic oxidation [11] are commonly used to fabricate nanostructure, but these methods are not suitable for zirconia ceramics because there are materials that are suitable for each processing method. Since zirconia is a hard and brittle material, it is difficult to mechanically process the surface directly. In addition, zirconia is resistant to conventional etching in the first place because of its chemical resistance [12]. Sriamporn et al. [13] created a micro/nanoscale porous surface by using a high-temperature solution for hydrofluoric acid (HF), which is inherently difficult to etch. However, tetragonal-to-monoclinic phase transformation was induced on the treated surface. Since YSZ mainly consists of tetragonal phases under atmospheric temperature and pressure conditions [14], this phase transformation changes the material properties of the substrate and may lead to a reduction in the strength and lifetime of the ceramics [15]. Sandblasting is a conventional process for creating rough surfaces, and these micro/nanoscale surface structures act as anchors to improve adhesion to other materials. However, it is difficult to control the processing location, and a deeper hole structure is considered suitable for support. In previous studies, an increase in the monoclinic ratio on the zirconia surface after sandblasting was reported, and damage to the material was a problem [16,17]. In another example, Bakkar et al. [18] processed YSZ with pore channels of several tens of nanometers in diameter by the freeze-casting process. It is possible to obtain sintered zirconia with nanostructures by using various sintering methods, but these methods can make the entire bulk porous.

Laser processing is one of the effective methods for creating nanostructures [19]. Many techniques have been studied to fabricate nanostructures, such as nanoholes and nanogrooves on the scale of several hundred nanometers or less, including: processing high aspect ratio nanoholes in SiO_2 substrates using femtosecond pulsed lasers [20–22]; fabrication of nanoholes, periodic nanostructures, and nanodot structures in metals using femto/picosecond pulsed lasers [23,24]; and drilling submicron holes in polymers using femtosecond pulsed lasers at extreme ultraviolet (XUV) wavelengths [25]. There are many reports on new nanostructure-processing methods and patterning that exceed the diffraction limit of laser light; however, to our knowledge, there have been no sufficient studies on polycrystalline zirconia for nanoholes, except for the formation of nanogrooves [26–28]. Therefore, in our previous study, we proposed a new method to fabricate nanoscale pores in YSZ. By irradiating the femtosecond pulsed laser, generation of nanopores in the crystal grains of the YSZ top layer succeeded [29]. A large number of pores can be generated on the surface with a single laser pulse irradiation without causing damage to the bulk by using this technique. These nanopores could be effectively used to load various materials on the YSZ surface and impart new functionalities.

Therefore, in this study, a novel method was proposed to embed material into nanopores formed in YSZ using laser irradiation. Figure 1 shows the structure of the target YSZ sample. First, a femtosecond pulsed laser was irradiated onto the polycrystalline YSZ substrate

to form nanopores within the surface crystal grains. Using the pose as an anchor, we attempted to create a functional material by locally filling and fixing any material within the nanopores. This nanopore structure is a new structure that we have realized, and the material has never been supported in the pores. If this method is realized, it can be expected to provide a new approach to surface functionalization for zirconia, which is difficult to microfabricate using conventional methods and suffers from damage during processing. Silver nanoparticles were selected as the embedding material. YSZ has excellent chemical stability and does not interact with silver, and silver has antibacterial properties [9], so YSZ has advantages in its use in biomaterials and daily necessities of people. For example, when implanted into the body as a biomaterial, YSZ's biocompatibility will allow it to bond well with bone and tissue, and the antibacterial and bactericidal effects of silver inhibit bacterial growth, increasing the stability of YSZ products. Since the base material is YSZ, excessive elution of metal ions and base material deterioration can be suppressed compared to metal base materials. In addition, the health risks associated with the absorption of silver ions are extremely low [30], and by introducing it into the pores, it can be expected to prevent desorption from the sample surface and provide a sustained effect. Furthermore, by generating pores at arbitrary locations on the surface, it becomes possible to selectively control the location where the material is supported. Material delivery systems have been actively studied in recent years [31], and if this technology, which takes advantage of the biocompatibility of YSZ itself, can be applied not only to silver but also to other materials, it may have further potential for application.
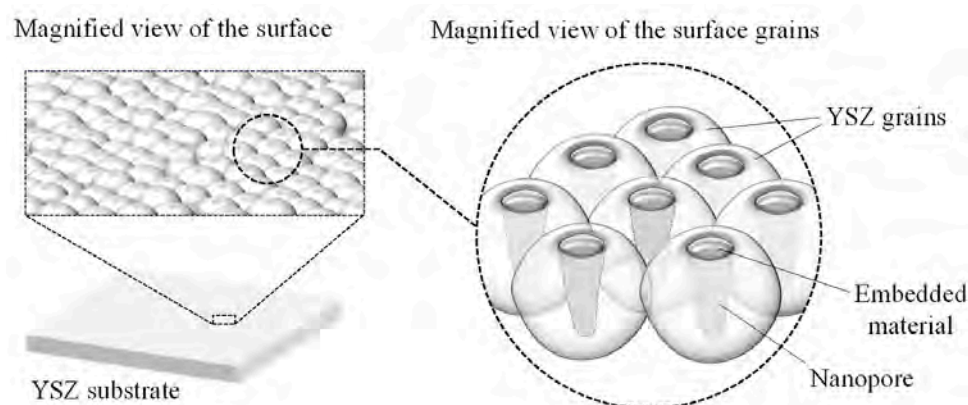

Figure 1. Surface nanopores with embedded silver nanoparticles.

Thus, in this study, the feasibility of metal nanoparticle loading into nanopores in zirconia surfaces by femtosecond pulsed laser irradiation, which has never been reported before, and the fundamental characteristics of the process were investigated. The laser irradiation conditions were varied, and the effects on the surface morphologies were clarified. The percentage of metal nanoparticles embedded in the pores and the structural change and processing damage of the zirconia substrate were also evaluated. The objective of this work is to create zirconia with nanopores embedding different material than the bulk using a laser irradiation process only. This study suggests a new approach for YSZ in various fields of industry by enhancing surface functionality. If a YSZ sample with silver nanoparticles embedded within the pores is realized, various applications can be expected based on the antibacterial properties, unique optical properties, high electrical and thermal conductivity, and nanomedicine delivery function of silver. Using this method, which uses a femtosecond pulsed laser that can minimize material damage, it is possible to obtain the effect of silver only on the surface while maintaining material strength, making it particularly suitable for YSZ, which is used as a biomaterial. Furthermore, by applying this method to other nanoparticle materials, it is expected that it will be possible to embed any material at any location on the surface and create YSZ surfaces with various desired functions.

2. Materials and Methods

Fully sintered YSZ polycrystalline doped with 3 mol% Y_2O_3 (Tosoh Corp., Tokyo, Japan) was used as the workpiece. Samples of rectangular plates with a thickness of 3 mm were prepared. The sample surface was sintered at 1500 °C and thermally etched at 1350 °C without polishing. The average grain size was 600 nm, and surface roughness was 309 ± 18 nm Ra. The entire workpiece was cleaned with acetone and ethanol before the experiment.

The Yb:KGW femtosecond pulsed laser (PHAROS-08-600-PP, Light Conversion, UAB, Vilnius, Lithuania) was used in this study. The laser parameters are summarized in Table 1. The laser wavelength was 1028 nm and the repetition frequency was 100 kHz. The laser spot diameter was 16 μm at the focal point. The laser beam had a Gaussian energy distribution, and laser beam scanning was controlled by a galvanometer scanner system in the X and Y directions. The beam was focused onto the workpiece placed on an adjustable z-axis stage through an fθ lens.

Table 1. Experimental conditions.

Parameters	(a) Nanopore Generation	(b) Fixation of Nanoparticles	(c) Fixation of Nanoparticles
Laser medium	Yb:KGW	Yb:KGW	Nd:YVO$_4$
Wavelength: λ [nm]	1028	1028	532
Spot size [μm]	16	16	85
Pulse width	256 fs	256 fs, 10 ps	26 ns
Repetition frequency: f [kHz]	100	100	100
Scanning speed: v [mm/s]	1000	10~500	53~1593
Laser power: E [mW]	450	60~140	1.7×10^3~4.0×10^3
Laser fluence: F [J/cm^2]	2.2	0.3~0.7	0.3~0.7
Number of scans: N	1	1	1
Atmosphere	Air	Air	Air

The schematics of the experimental process are shown in Figure 2. Firstly, a laser was irradiated on the entire sample surface to generate nanopores by using laser parameters summarized in Table 1 (a). Then, nano-silver dispersion liquid (Japan Ion Corp., Tokyo, Japan) was dropped onto the surface. The workpiece was dried in a vacuum desiccator for 24 h to completely remove moisture from the surface to avoid hydrothermal degradation caused by contact between zirconia and water molecules [32]. To embed silver nanoparticles in the nanopores and remove excessive deposits simultaneously, the laser beam was scanned again on the workpiece. To investigate the nanoparticle embedding characteristics, the laser beam was scanned for various laser fluences, scanning speeds, and pulse widths summarized in Table 1 (b). To remove the excess dried film of the dispersion attached to the outside of the pore without processing the original YSZ surface, the laser fluence was set extremely smaller than the ablation threshold of zirconia to selectively remove only the target material from the surface. For the comparison, the Nd:YVO$_4$ nanosecond pulsed laser (Super Pulse 532-30, Inngu Laser Co., Ltd., Zhengzhou, China) and electric furnace (High-performance muffle furnace HPM-1N, AS One Corp., Osaka, Japan) were used to remove the excess dried film. The nanosecond pulsed laser was irradiated with various laser parameters summarized in Table 1 (c). Since the beam diameter was different from the femtosecond pulsed laser, the scanning speed was adjusted so that the pulse overlap rate was the same. On the other hand, the workpiece was heated in an electric furnace at 450 °C for 30 min in air. All experiments in this study were performed under atmospheric conditions.
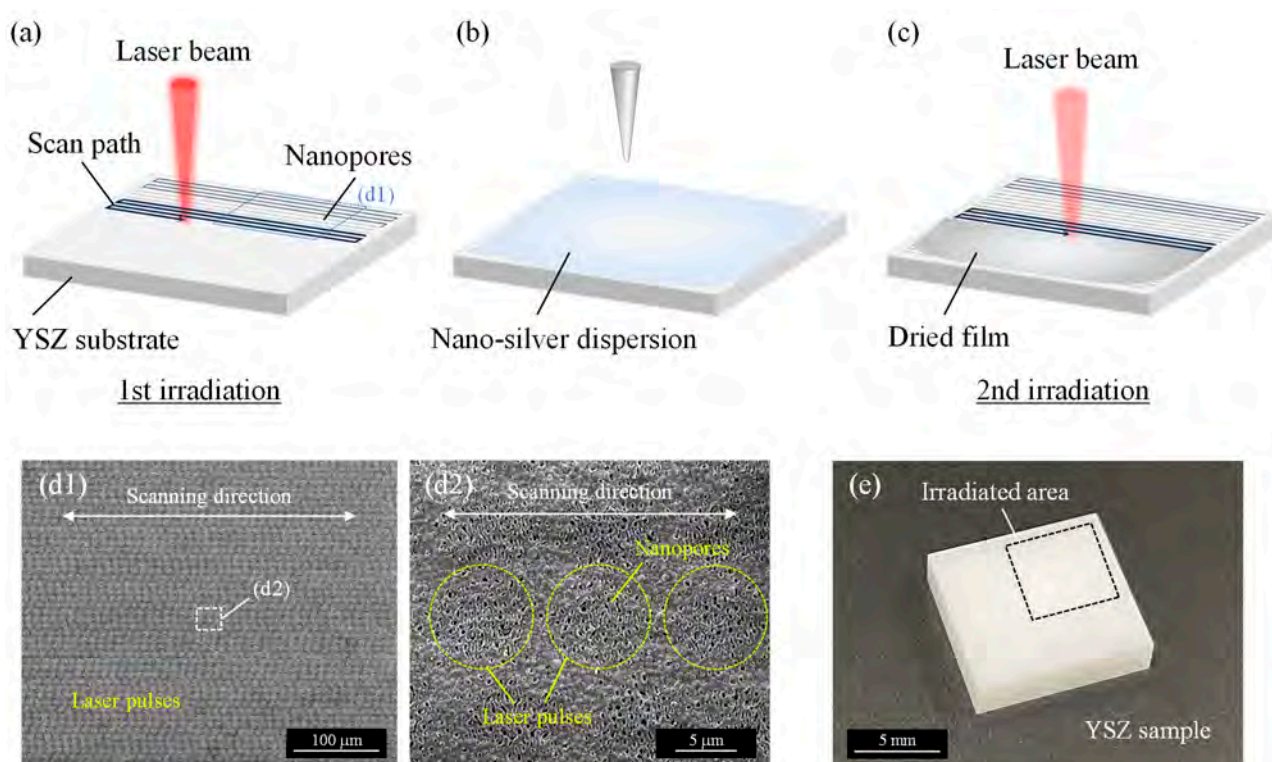
Figure 2. Schematics of experimental procedure: (**a**) nanopore fabrication on entire YSZ surface by irradiating femtosecond pulsed laser; (**b**) nano-silver dispersion liquid is dropped onto the surface and dried in a vacuum desiccator; (**c**) laser irradiation is used to embed nanoparticles and remove excess dried film; (**d**) SEM images of irradiated surface in process (**a**); (**e**) overview of YSZ sample.

To observe silver nanoparticles in nano-silver dispersion, a field-emission transmission electron microscopy (FE-TEM, Tecnai G2, FEI Co., Hillsboro, OR, USA) was used. The nano-silver dispersion was dropped onto a glass plate and completely dried in a desiccator by removing the water. The remaining dried film was then shaved off from the glass plate with a razor blade and finely ground in a mortar for TEM observation. To measure the size distribution of silver nanoparticles, the diameters of four hundred particles were measured from a TEM image using image analysis software ImageJ (version 1.53; U.S. National Institutes of Health, Bethesda, MD, USA).

After nanopore generation, a zeta potential analyzer (ELS-Z2PT, Otsuka Electronics Co., Ltd., Tokyo, Japan) was used to measure the zeta potential of nano-silver dispersion and the YSZ surface, and pH was measured with a pH meter (pH METER D-51, HORIBA Ltd., Osaka, Japan). After the irradiating laser to remove the excessively dried film, the surface morphologies of the irradiated sample were observed by a field-emission scanning electron microscope (FE-SEM, Inspect F50, FEI Co., Hillsboro, OR, USA). An energy-dispersive X-ray spectroscopy (EDX, EDAX Inc., Pleasanton, CA, USA) was used to analyze the elemental distribution. For the cross-sectional investigation of pores, a focused ion beam system (FIB, Quanta 3D 200i, FEI Co., Hillsboro, OR, USA) was used to cut the sample. An FE-SEM (ZEISS GeminiSEM 500, Carl Zeiss AG, Oberkochen, Germany) was also used to observe the cross-section of the pore. Elemental distribution under the irradiated surface was investigated by glow discharge optical emission spectroscopy (GDOES, GD-Profiler2, HORIBA Ltd., Osaka, Japan). Moreover, the material phase structure was evaluated by a laser micro-Raman spectrometer (InVia Raman Microscope, Renishaw plc., Kingswood, UK) with a laser wavelength of 532 nm and a beam diameter of 1 µm.

For the quantitative evaluation, the number of pores with and without embedded material was counted. Nine SEM images of the same field of view at 40,000× were prepared for each irradiation condition. The ratio of the number of pores with implantation to the

total number of pores in the field of view was defined as the "pore-embedded ratio", and the average value for nine images was calculated.

3. Results and Discussion

3.1. Characteristics of Nano-Silver Dispersion

The basics of nano-silver dispersion used in this study were investigated as shown in Figure 3. After removing the water from the dispersion, a large matrix made of polyvinylpyrrolidone (PVP) polymer which was water soluble and originally included as a dispersant in the nano-silver dispersion was observed, and countless nanoparticles were contained in the PVP as shown in Figure 3a. According to EDX analysis, these nanoparticles were indeed silver (Figure 3b,c). TEM images showed that the silver nanoparticles were spherical and varied in diameter from a few nm to about 10 nm (Figure 3d). In addition, individual nanoparticles were dispersed and did not aggregate to form large clumps that would prevent entry into the pore. It is thought that the silver nanoparticles originally existed in a dispersed state in the nano-silver dispersion liquid without aggregation due to the effect of PVP and that the removal of water from the dispersion fixed the nanoparticles in a dispersed state in the dried PVP film. The particle size distribution chart showed that the mode was 3.5 nm and the average diameter was 4.6 ± 2.0 nm (Figure 3e). This indicates that the silver nanoparticles were sufficiently smaller than the nanopores, which were approximately 100 nm in diameter. Therefore, the silver nanoparticles are fully capable of entering the nanopore.
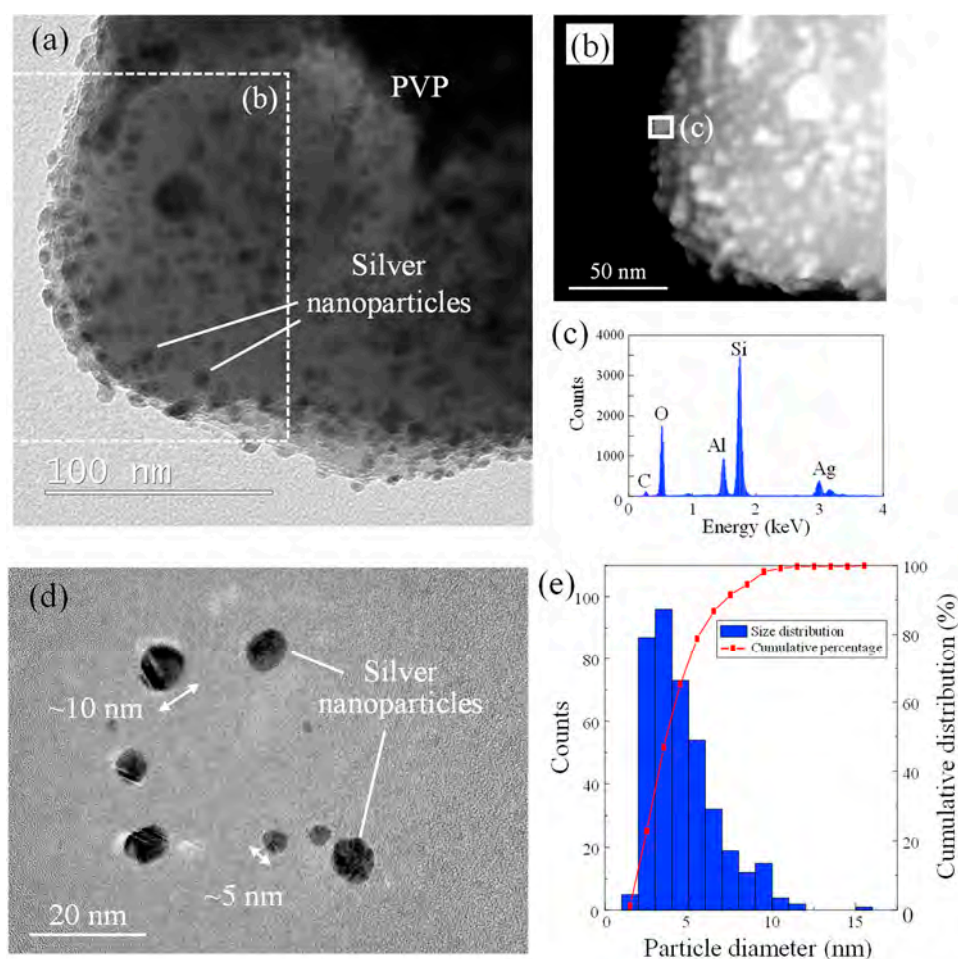

Figure 3. (**a**) TEM image of dried nano-silver dispersion, (**b**) HAADF-STEM image of dried nano-silver dispersion, (**c**) EDX spectra of silver nanoparticle in PVP matrix, (**d**) TEM image of silver nanoparticles separated from PVP matrix, (**e**) size distribution of silver nanoparticle.

It is necessary to investigate whether the nanoparticles adsorb on the substrate after dropping the dispersion on the YSZ surface. The driving force for the adsorption of nanoparticles on the YSZ substrate could be the Coulomb force due to the surface charge of the YSZ and silver nanoparticles. Figure 4 shows the zeta potential of each sample. At the expected dilution ratio, the pH of the dispersion was about 5.0~5.8 (Figure 4a). In this pH range, the YSZ surface after nanopore generation showed a slightly positive zeta potential, and nano-silver dispersion showed a negative zeta potential (Figure 4b). The polarity of the surface charge of silver nanoparticles in the dispersant and YSZ surface was opposite, indicating that the nanoparticles were in a desirable state to adsorb onto the sample.
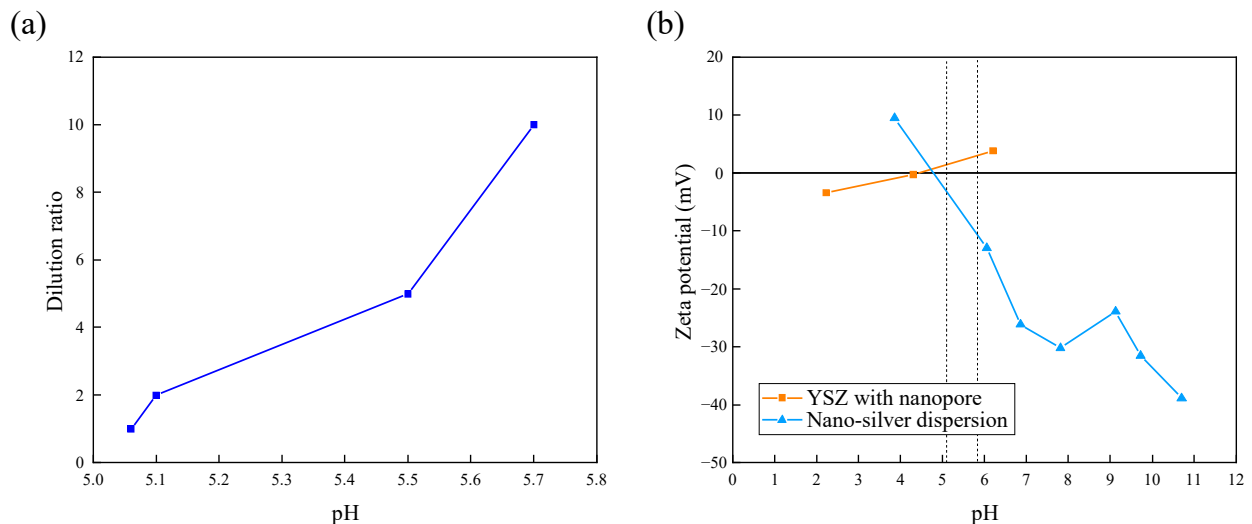
(a)

(b)

Figure 4. (**a**) Relationship between water dilution ratio and pH; (**b**) change in zeta potential of each sample. (The two dashed lines indicate the pH range of the water in (**a**)).

3.2. Surface Morphology

3.2.1. Effect of Laser Fluence and Scanning Speed

After the nano-silver dispersion was applied to the pore-processed surface, the processing characteristics of the second laser irradiation (Figure 2c) were evaluated. To investigate the effect of the laser conditions, line irradiation was conducted. The laser beam was scanned a single time at a pulse width of 256 fs with different laser fluences and scanning speeds. Figure 5 shows the SEM images of the irradiated surface at a scanning speed of 10 mm/s with various laser fluences. From low magnification images (Figure 5(a1–c1)), the dried dispersion film was completely removed at the laser-scanned area and the YSZ surface with pre-processed nanopores was exposed. At $0.4 \, J/cm^2$ and $0.5 \, J/cm^2$, only dried film was removed from the surface; however, by increasing laser fluence to $0.7 \, J/cm^2$, the YSZ substrate was also machined and the surface with nanopores was partially peeled off. In general, the ablation threshold for YSZ is larger than $0.7 \, J/cm^2$, but it is thought that the roughening of the surface due to nanopore formation would cause processing even at smaller fluences. Therefore, the surface tended to be more removed in the pore-generated area than in the unprocessed area.

From high-magnification images, it was clear that many nanopores kept their shape after laser irradiation and were filled with some material at $0.4 \, J/cm^2$ (Figure 5(a2)). When the laser was irradiated at $0.5 \, J/cm^2$, periodic structures were partially formed around the apertures of pores (Figure 5(b2)). At $0.7 \, J/cm^2$, the periodic structures formed a larger area, and the grain surface also had periodic spallation marks (Figure 5(c2)). These structures were considered to be the laser-induced periodic surface structures (LIPSS) that form by irradiating ultrashort laser pulses near the ablation threshold [33]. In general, LIPSS are classified into two types based on their periodicity. LIPSS with a period on the same scale as the irradiated laser wavelength are low-spatial frequency LIPSS (LSFL), and those with

a period of less than half of the wavelength are high-spatial frequency LIPSS (HSFL). In this study, LIPSS were formed perpendicular to the laser polarization direction, and the periodicity was approximately 100~200 nm, which was much smaller than half of the laser wavelength ($\lambda/2$ = 514 nm). This indicates that the structures were HSFL. In general, LIPSS have advantages in improving and enhancing surface functionalities such as wettability, biocompatibility, and wear resistance, and have a wide range of applications [34,35]. Our previous study also revealed that LIPSS formation enhances the hydrophilicity of the YSZ surface [26]. However, in this study, the irradiation condition where clear LIPSS formed (Figure 5c) resulted in the removal of silver and surface layers. Change in pore diameter irradiated with different fluences was measured, as shown in Table 2. As a result, there was no change in pore diameter due to changes in laser fluence. It was shown that surface processing such as LIPSS occurred around the pore as the fluence increased, but it did not affect the size or shape of the pore itself. According to these results, the material different from the substrate was successfully embedded only within the pre-made nanopore by laser process by adjusting irradiation conditions. It was also found that lower laser fluence can suppress surface damage such as LIPSS formation and removal of the surface layer of YSZ substrate to retain nanopore shape.
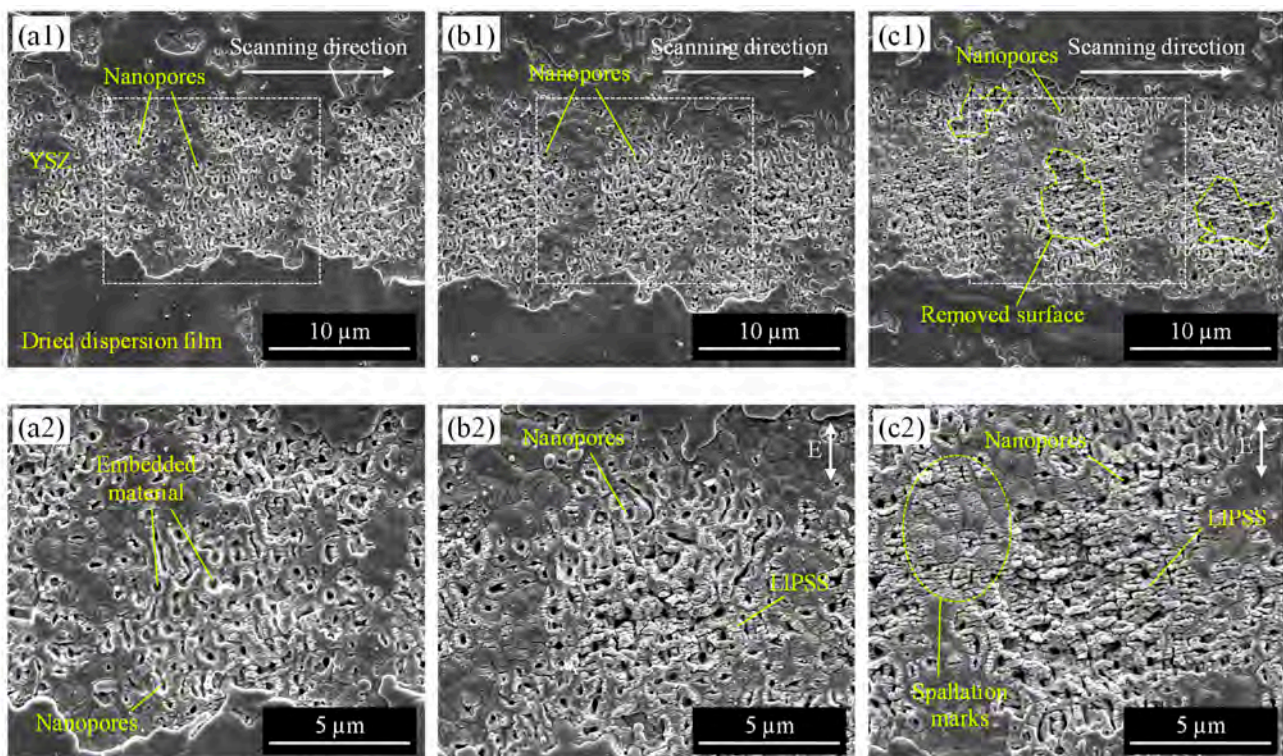

Figure 5. SEM images of the irradiated surface at a scanning speed of 10 mm/s with varying laser fluence: (**a**) 0.4 J/cm^2, (**b**) 0.5 J/cm^2, (**c**) 0.7 J/cm^2; (**a1**–**c1**) are low-magnification images, and (**a2**–**c2**) are high-magnification images.

Table 2. Pore size on irradiated YSZ surfaces in Figure 5.

Parameters	(a) 0.4 J/cm^2	(b) 0.5 J/cm^2	(c) 0.7 J/cm^2
Average pore diameter [nm]	125 ± 21	122 ± 16	128 ± 20

The effect of laser scanning speed was investigated. Figure 6 shows the SEM images of the irradiated surface at a laser fluence of 0.5 J/cm^2 with various scanning speeds. At low scanning speed, dried film was completely removed at the irradiated area (Figure 6a). When the scanning speed increased, the removed area also decreased due to the decrease in

laser pulse overlap (Figure 6b). At high scanning speed, the dried film swelled into a tunnel-like shape, some top parts partially remained, and some were peeled off (Figure 6c). Under the swelled film, nanopores with embedded materials were observed. It is considered that the surface was expanded due to the heating effect of laser irradiation since the dried film was mainly PVP polymer containing silver nanoparticles. It was reported that when the resin surface was irradiated by a femtosecond pulsed laser, the resin expanded and decomposed near the surface, and then a cavity was formed [36]. It has also been reported that increasing the fluence in laser ablation causes the thermal stress difference between the substrate and the coating film to be greater than the adhesive force between the two, causing the coating film to delaminate [37]. Thus, in this study, the film expanded and decomposed, and the internal pressure between the surface film and the YSZ substrate increased, which is thought to have caused the top surface of the film to delaminate.
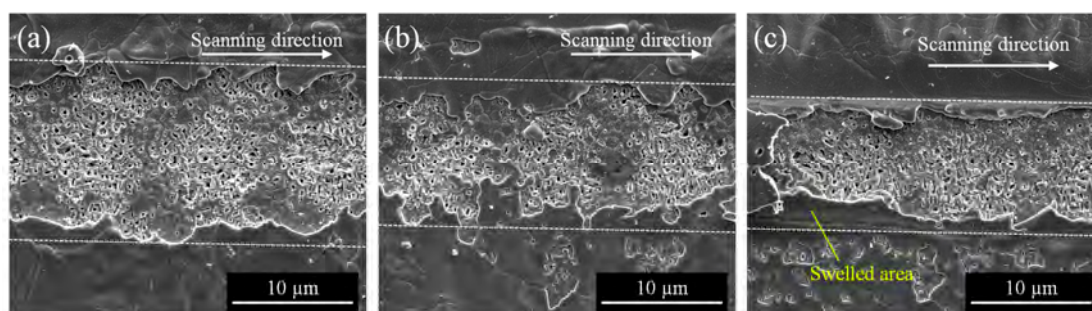

Figure 6. SEM images of the irradiated surface at a laser fluence of 0.5 J/cm^2 with varying scanning speed: (**a**) 10 mm/s, (**b**) 100 mm/s, (**c**) 200 mm/s.

To investigate the elemental component of the irradiated surface, elemental mapping by EDX was performed. The sample was prepared by area irradiation with a laser fluence of 0.5 J/cm^2, a scanning speed of 200 mm/s, and a scan pitch of 8 μm. Figure 7 shows an SEM image and elemental map of the nanopores. Many yellow dots indicating silver (Ag) were observed on the surface corresponding to the area where the pore formed. In addition, microscale debris adhered around the pores also showed silver and carbon (C). It is considered that the carbon was derived from the PVP in nano-silver dispersion, indicating the microscale debris was dried PVP containing silver nanoparticles. By extracting PVP microscale debris adhering to the YSZ surface from the SEM image after laser irradiation using image analysis, the PVP removal rate, i.e., the area ratio to the irradiated surface, was calculated. The PVP debris was found to be only about 1% of the YSZ surface area, indicating that most of the PVP was removed. To effectively remove residual PVP, the pitch spacing at which the laser scans is considered to be important. If the pitch spacing between each irradiated line is too wide, unirradiated areas may occur and PVP may not be fully removed.

To clarify the positional relationship between the distribution of silver and the nanopores on the YSZ surface, a distribution map was made by image analysis software, as shown in Figure 7c. The orange color represents the nanopores extracted from the SEM image (Figure 7a), and the blue color represents the distribution of silver detected in Figure 7b. The nanopores were densely distributed in a circular region corresponding to the laser pulse shape. Silver was also distributed corresponding to the pulse shape where the pores were concentrated, and was almost uniformly distributed within the circular region. There was almost no silver adhered to the gaps between the pulses where almost no pores were formed, i.e., the unprocessed area. This suggests that silver is uniformly distributed in the pore-generated area and that the pores act as anchors to hold the silver. Hence, according to the above results, it was found that silver nanoparticles were successfully embedded and remained in the nanopores after laser irradiation. Furthermore, the dried PVP film on the irradiated surface outside the nanopores was found to be removed by the laser.
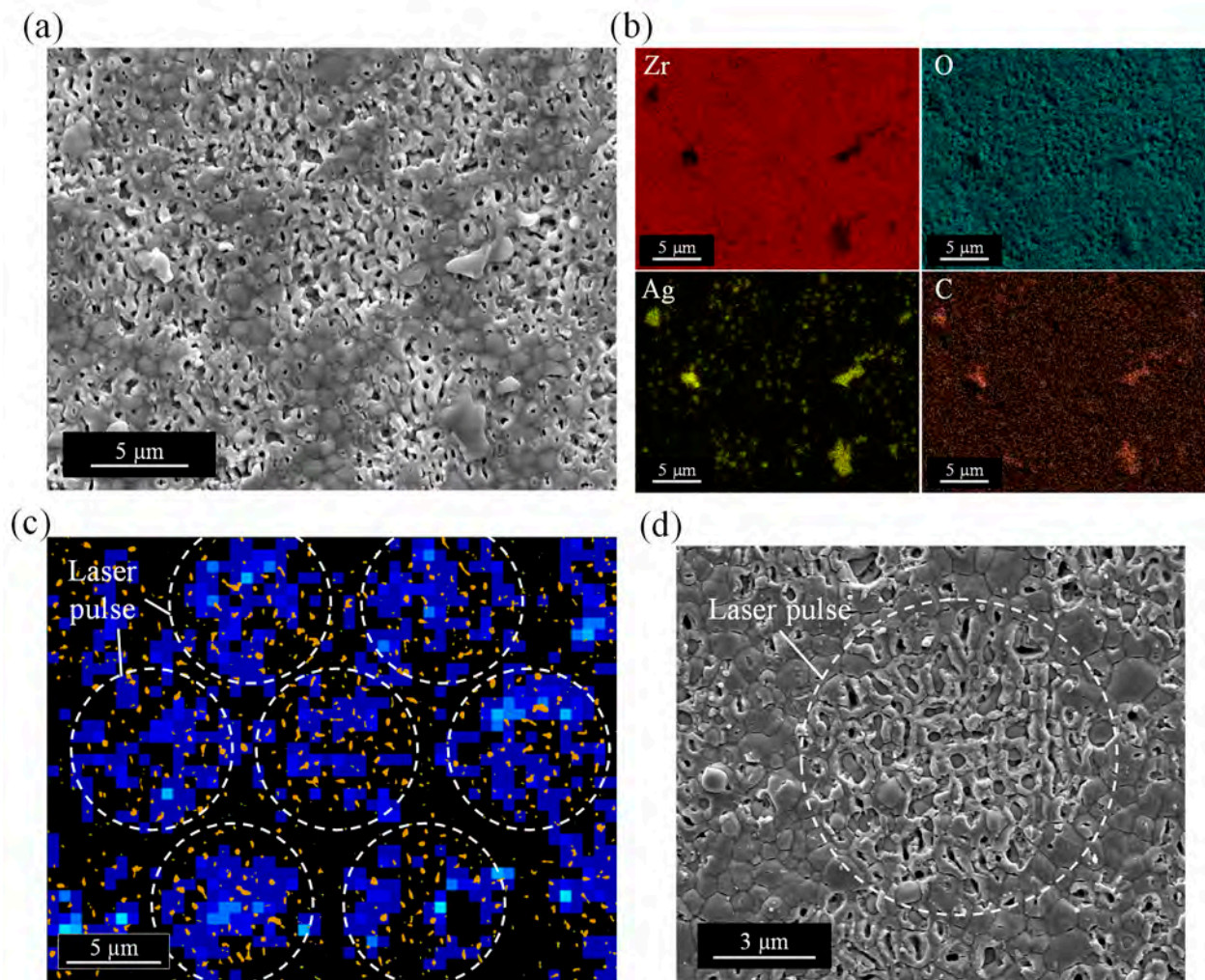
Figure 7. EDX analysis of YSZ surface after embedding silver nanoparticles by laser irradiation: (**a**) SEM image, (**b**) elemental mapping images, (**c**) distribution map of nanopore (orange color) and silver (blue color), (**d**) magnified image of silver-embedded nanopore surface.

3.2.2. Effect of Pulse Width

Thermal effects in the laser process are also considered to be an important factor in removing excess PVP on the surface and implanting silver nanoparticles in the pore. To investigate the effect of the pulse width which significantly affects the thermal effect during the process, line irradiation was performed on the YSZ surface using three different pulse widths: femtosecond (fs), picosecond (ps), and nanosecond (ns). The scanning speed was adjusted to become the same pulse overlap rate for each laser. The SEM images of the irradiated surface at different parameters are shown in Figure 8. When irradiated with low laser fluence (Figure 8(a1–c1)), there were many embedded nanopores on the YSZ surface at 256 fs. Materials in the pore were still observed at 10 ps. On the other hand, they were completely removed after irradiating nanosecond pulses of 26 ns. White-colored spheres with diameters on the order of hundreds and tens of nanometers were densely adhered to the surface of the original grains around the pores. When irradiated with high laser fluence (Figure 8(a2–c2)), LIPSS were formed on the surface, and almost no embedded materials were in the pores at 256 fs. By increasing pulse width to 10 ps, LIPSS formation was suppressed and only the aperture of the pore split, keeping materials in the pore. At 26 ns, the YSZ surface was melted and each grain was difficult to identify. Some microcracks were also generated along the original grain boundaries. No residue remained in the pores, but very small particles were attached to the surface.
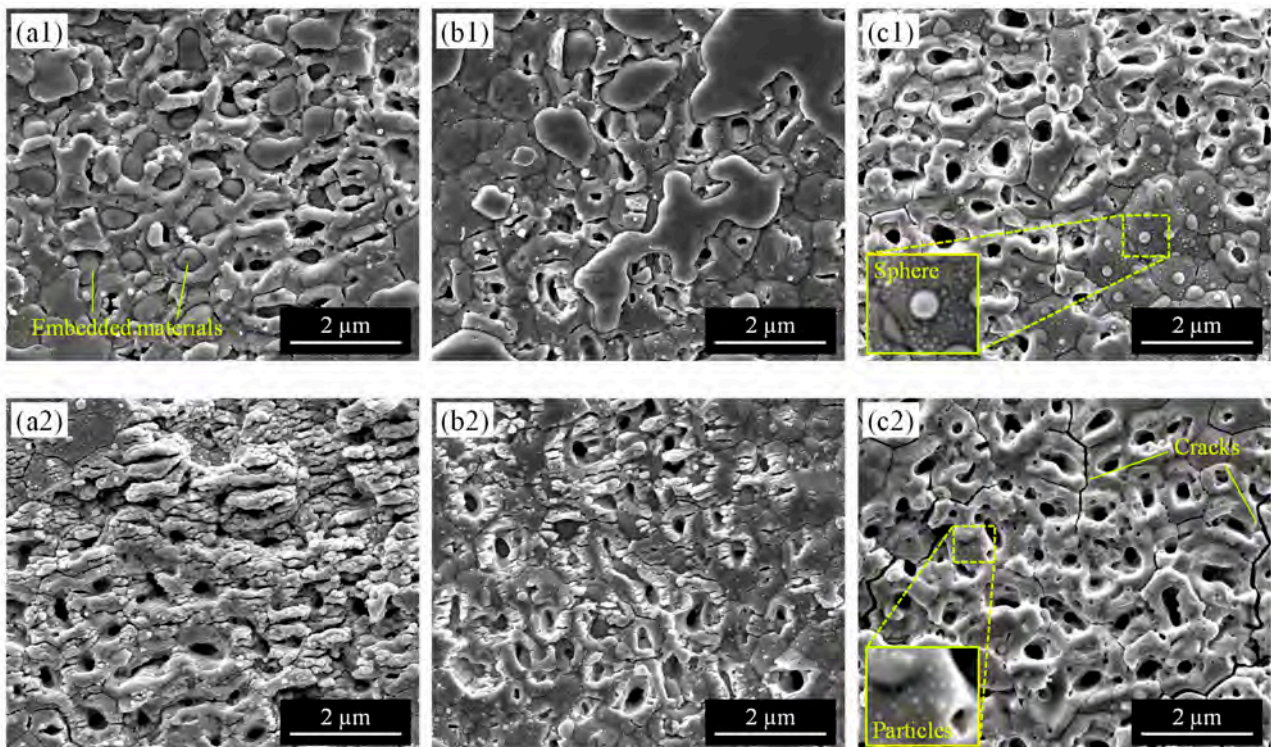
Figure 8. SEM images of the irradiated surface with varying pulse width: (**a**) 256 fs (10 mm/s), (**b**) 10 ps (10 mm/s), (**c**) 26 ns (53 mm/s). (**a1**–**c1**) are irradiated at laser fluence of 0.3 J/cm^2, and (**a2**–**c2**) are irradiated at laser fluence of 0.7 J/cm^2.

To compare differences in PVP response due to thermal effects, a sample was heated in an electric furnace at 450 °C to remove surface deposits instead of using a laser. The heating temperature was set to slightly exceed the decomposition temperature of the PVP. Figure 9 shows the surface morphology of the sample. Figure 9a shows many spheres attached to the YSZ surface, and their size seemed quite larger than those observed on the surface irradiated by a nanosecond pulsed laser (Figure 8c). By the backscattered electron (BSE) image of Figure 9b, the spheres were detected in a brighter color than the YSZ substrate, which indicates that it is composed of heavier elements than zirconium, i.e., silver without PVP. It was found that all of the larger silver spheres were attached to the pore-forming region but did not penetrate the interior of the pore. The results in Figures 8 and 9 suggest that laser processing, with a shorter pulse width, is suitable for implantation into the pore, rather than simply heating the surface.
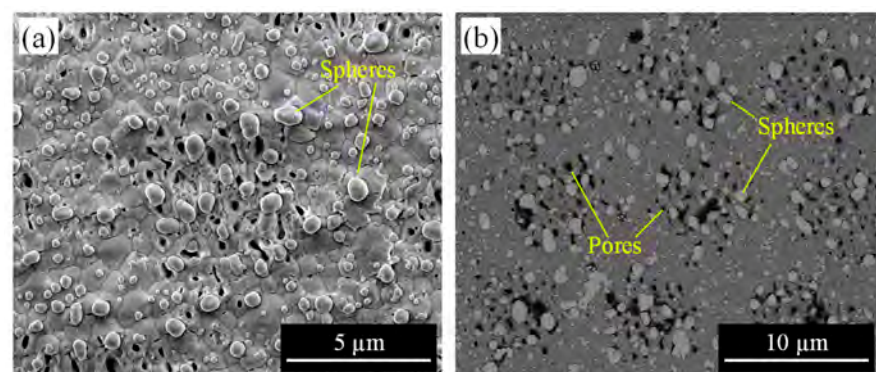

Figure 9. YSZ surface after heating in an electric furnace: (**a**) secondary electron (SE) image, (**b**) backscattered electron (BSE) image.

According to the abovementioned results, the surface morphology of dried nano-silver dispersion film and YSZ substrate after laser irradiation under different parameters were summarized. Figure 10 shows parameter maps. The range of the scanning speed in each graph was unified so that the overlap rate was the same. At 256 fs, the dried film was able to be removed in a limited range of laser fluence and scanning speeds. There was a tendency for the laser beam not to affect the surface at a higher scanning speed for each laser fluence, and the YSZ surface structure changed to LIPSS at a lower speed. The range of conditions in which film was removed was further reduced by increasing pulse width. Although the dried film could be removed at longer pulses such as 26 ns, the YSZ surface was damaged. Therefore, the ultrashort pulse is suitable for this silver nanoparticle-embedded process proposed in this study.
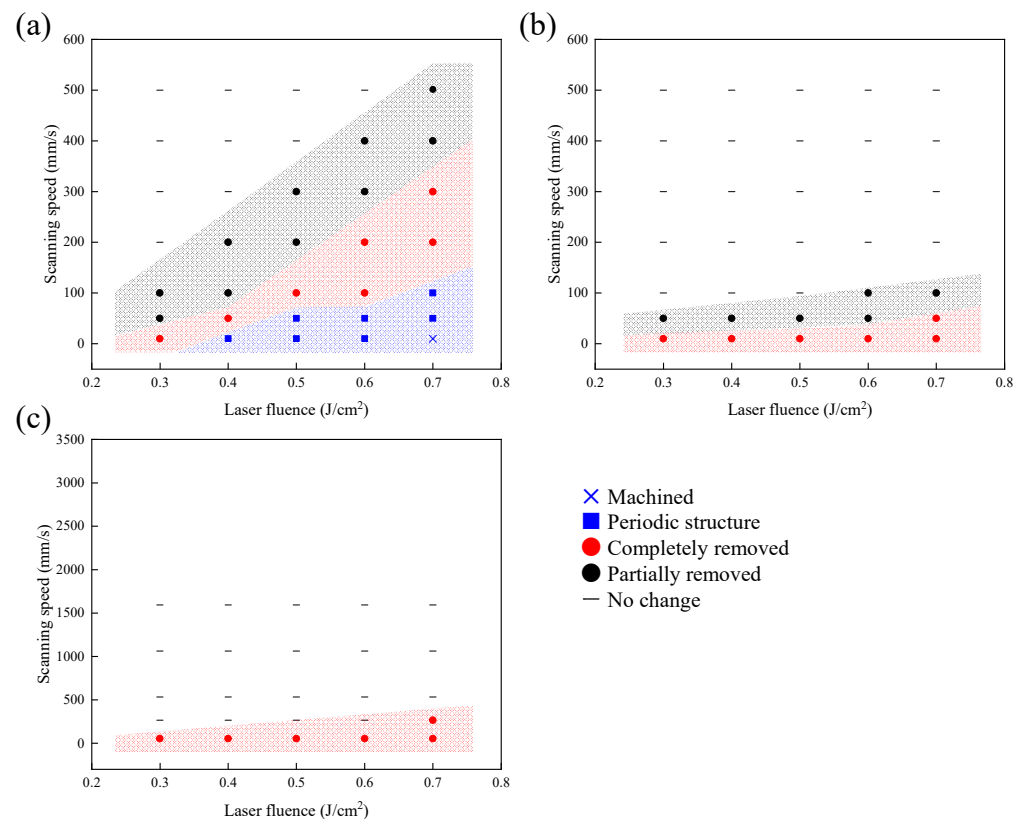

Figure 10. Parameter map of dried nano-silver dispersion film and YSZ surface morphology irradiated at the different pulse widths: (**a**) 256 fs, (**b**) 10 ps, (**c**) 26 ns.

3.3. Pore-Embedded Ratio

For quantitative analysis of silver implantation, the pore-embedded ratio of the laser-irradiated surface with different laser fluences and scanning speeds was evaluated. Figure 11 shows the change in the pore-embedded ratio when irradiated by femtosecond pulsed laser at 256 fs. A pore-embedded ratio of around 60% was achieved in this study. It was found that there were different laser fluences for each scanning speed, which showed the best pore-embedded ratio; for example, 0.3 J/cm^2 showed the highest value at 10 mm/s, whereas 0.4 J/cm^2 was the highest at 50 mm/s, and 0.5 J/cm^2 was the highest at 100 mm/s. It seems that the highest value for each scanning speed did not significantly differ. Thus, it was concluded that the combination of both two laser parameters was important.

To understand the change in pore-embedded ratio in more detail, the result of Figure 11 was summarized in a color distribution map. Figure 12 shows the color map overlaid on the parameter map shown in Figure 10a. It was found that materials were embedded in nanopores at the laser condition where the dried film was partially peeled off and where LIPSS were generated. In the parameter range where the dried film was completely

removed from the surface, a higher pore-embedded ratio was obtained, up to approximately 60%. In the range where LIPSS were observed, the pore-embedded ratio tended to decrease. Especially when the fluence was increased at low scanning speeds, the embedding rate was low because the YSZ substrate surface with silver-loaded pores was processed.
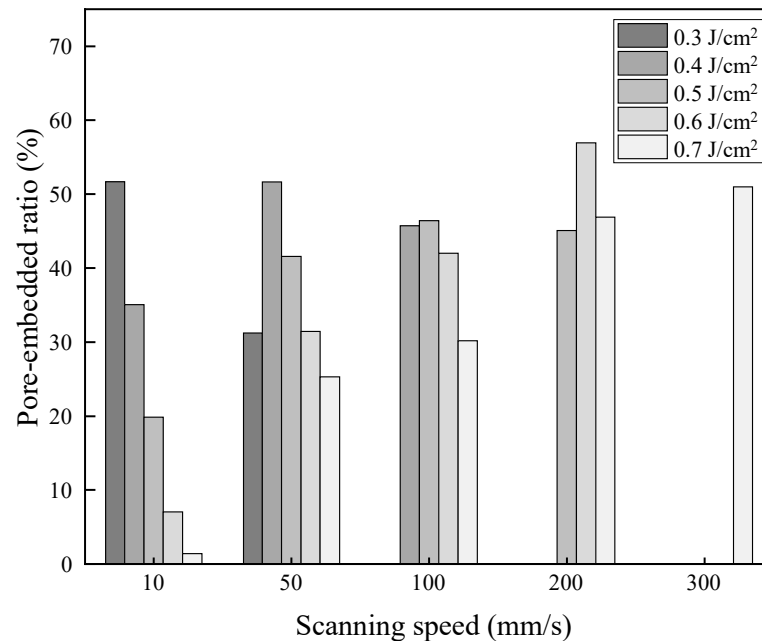

Figure 11. Change in pore-embedded ratio with different laser fluences and scanning speeds.

3.4. Cross-Sectional Structures

To investigate the embedded material in the pores in detail, cross-sectional observation was conducted. Figure 13a shows the backscattered electron (BSE) image of the cross-section of pores irradiated with a laser fluence of 0.5 J/cm^2, a scanning speed of 200 mm/s, a scan pitch of 8 μm, and a pulse width of 256 fs. There was some clumping inside the pores, and the material was embedded to the deepest depth in all of the pores. The clumps were detected in a brighter color than the YSZ substrate, indicating that they may be heavier elements than zirconium, i.e., silver. To clarify the elemental component, the EDX mapping of each element is shown in Figure 13b. YSZ substrate consisted of zirconium (Zr) and yttrium (Y); however, it was not in the area of nanopores. It was found that the pores were filled with silver (Ag), and silver completely penetrated inside the pore. Outside the pore, i.e., the YSZ surface, had no bright silver peak, indicating the attached material on the surface was selectively removed by laser irradiation keeping the silver inside the pore. A small amount of carbon (C) was detected around the nanopore apertures. On the other hand, no carbon was observed in the area inside the pore where the clear silver peak was detected, indicating that the silver and the dispersant, PVP, were completely separated in the pore. In addition, almost no oxygen was detected inside the pores, and it could not be determined that the silver clumps were severely oxidized. Moreover, no elements other than the constituent elements (Zr, O, Ag, and C) were detected in the cross-sections, except for elements attributed to the Pt coating and the measurement device.
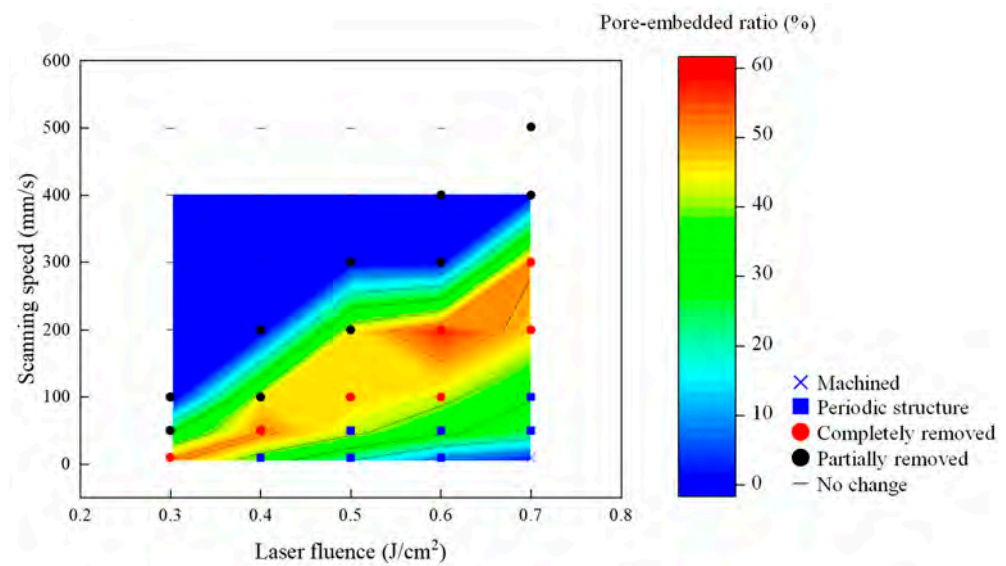
Figure 12. Parameter map with a color map of the change in pore-embedded ratio irradiated with the pulse width of 256 fs.
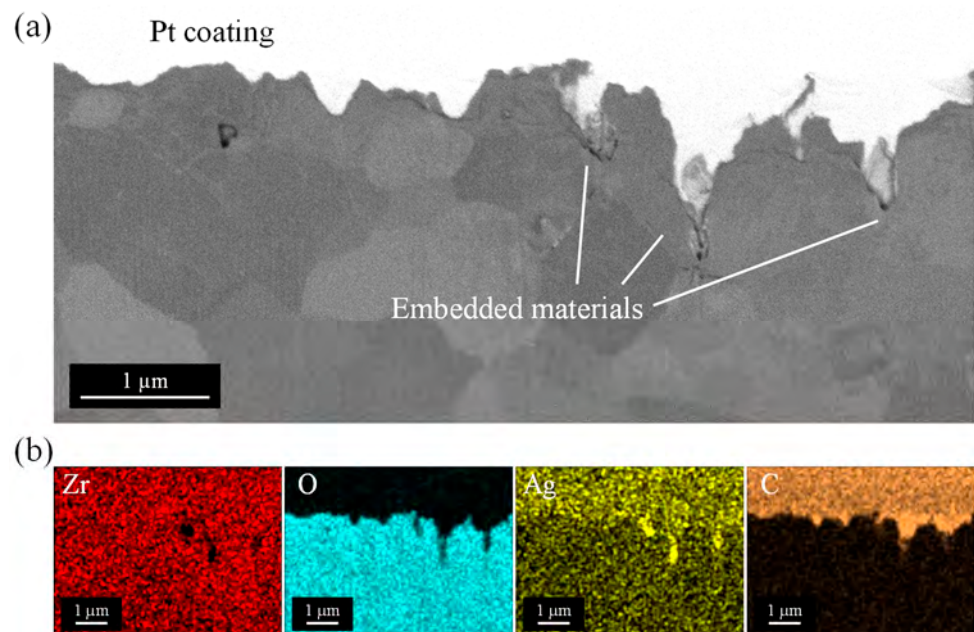

Figure 13. EDX analysis of the cross-section of the pores after embedding silver nanoparticles: (**a**) Backscattered electron (BSE) image, (**b**) elemental mapping images.

Elemental distribution in the depth direction of the sample was investigated by GDOES analysis. The sample was prepared by area irradiation with a laser fluence of 0.5 J/cm^2, a scanning speed of 200 mm/s, a scan pitch of 8 μm, and a pulse width of 256 fs. Figure 14 shows the distribution of each chemical component with depth from the sample surface. After laser treatment, no significant changes with depth from the surface in the main components of YSZ such as zirconium (Zr), oxygen (O), and yttrium (Y) were observed (Figure 14a). This is considered to be an effect of ultrashort pulse irradiation. Femtosecond pulsed laser irradiation is characterized by its ability to suppress thermal effects on surrounding materials by irradiating high-intensity energy in an extremely short time. In addition, since the objective of this study was to remove the dried film on the surface and embed silver nanoparticles, a laser fluence extremely smaller than the ablation threshold of YSZ was used. Therefore, even though the laser irradiation removed the dried

film, which has a smaller ablation threshold than YSZ, the surface of the YSZ substrate itself did not melt. Hence, there is no risk of segregation of certain components such as yttria in the material, and as a result, the components in the original sample remained unchanged. After laser treatment, a small amount of carbon (C) was also detected and slightly increased at depths less than 200 nm, but almost zero in other areas. The amount of carbon on the top layer was smaller than that found on the sample surface after nanopore fabrication, where all surface organic materials were completely removed by ablation [29], indicating that the most of PVP dispersants in the nano-silver dispersion were removed by the laser treatment, and residual PVP, identified in EDX mapping results (Figures 7 and 13), was almost negligible. For the detailed analysis, silver (Ag) was extracted from the graph, as shown in Figure 14b. Silver significantly increased as the surface was approached. It seems that silver existed at the depth in the range from 600 nm to 800 nm, and this value corresponded well to the grain size of the sample. Our previous study showed that localized energy absorption within the grains of the top layer of the YSZ results in the formation of long-elongated nanopores form within the grains. Pore size depends on the zirconia grain size, and thus the maximum depth of the pore also corresponds to the grain size. Therefore, the fact that silver was detected in the GDOES analysis to the same depth as the grain size of the sample indicates that silver has reached the deepest part of the pre-fabricated nanopores. In addition, the result that the silver peak gradually decreased within the range of the grain size of the surface grains indicates that silver was present without extreme bias from the top to the deepest point in the nanopore. This indicates that the silver in the pore was not removed by laser treatment with appropriate irradiation conditions and that the pore was filled to the deepest part. The measurements were taken over a wide area, approximately 40 mm in diameter, of a sample that had pores on the entire surfaces. Hence, it can be said that in all areas, silver nanoparticles firmly penetrated the bottom of the pores and still remained after laser treatment.
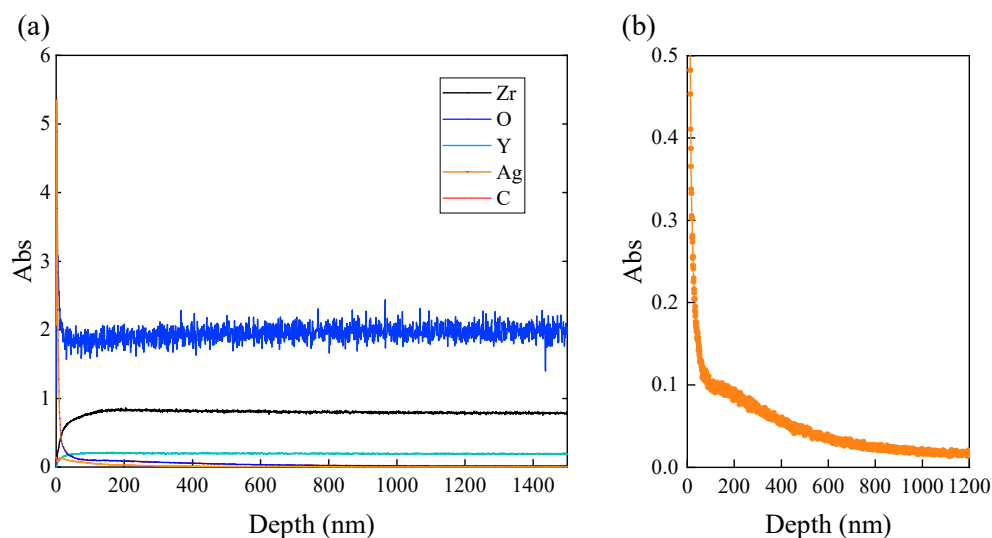

Figure 14. GDOES analysis of YSZ surface after embedding silver nanoparticles in the nanopores: (**a**) GDOES depth profile for each element, (**b**) magnified depth profile of Ag.

3.5. Material Phase Analysis

To investigate the thermal damage of YSZ during the laser process, the material phase before and after laser irradiation was measured. Figure 15 presents the Raman spectra of the exposed YSZ surface after the removal of the surface dispersion film by various methods. A sample heated in an electric furnace to remove surface deposits instead of using a laser showed many characteristic peaks. Large monoclinic (m) peaks appeared between tetragonal (t) peaks compared to the unirradiated original YSZ surface [38], indicating that the phase transformation of YSZ from tetragonal to monoclinic phase progressed remark-

ably during the heating process. When the dried film was removed by laser irradiation, the monoclinic peaks were not as distinct as those observed on the surface after electric furnace heating, whether femtosecond, picosecond, or nanosecond pulse widths were used. This result was not changed by changing the laser fluence of the femtosecond laser pulses. The samples after the surface treatment all showed a large leftward spectral increase of around 50 cm^{-1}. In the Raman analysis, when a strongly scattering material is measured, the low wavenumber side of the spectrum rises due to the effect of laser scattering. In this study, silver nanoparticles adhered to the surface after laser irradiation and heating in an electric furnace, which may have affected the spectral measurements. Although this spectral increase may have hidden the original zirconia peaks, it is clear that no significantly larger monoclinic peaks appeared compared to the furnace-heated surface.
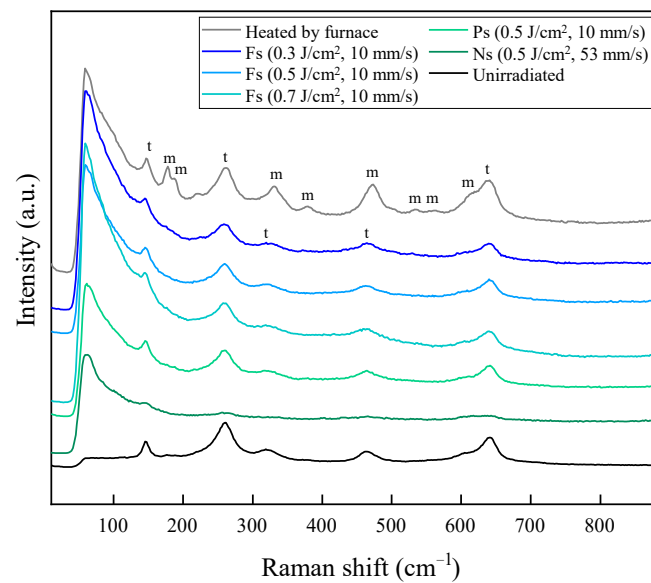

Figure 15. Raman spectra of the before and after irradiated surface with different laser parameters, showing monoclinic (m) and tetragonal (t) peaks.

For quantitative analysis, the monoclinic volume ratio was calculated by the Raman intensity method [39]. The integrated intensity I of three peaks (147 cm^{-1}, 181 cm^{-1}, and 190 cm^{-1}) from the baseline determined by connecting the minimum points of each peak was measured, and the monoclinic ratio V_m was calculated by following the equation:

$$V_m = \frac{I_m(181) + I_m(190)}{2.07 \times I_t(147) + I_m(181) + I_m(190)} \tag{1}$$

where the subscripts m and t identify the monoclinic and tetragonal phases, respectively. The monoclinic ratio of the furnace-heated surface was about 36%, while the other laser-irradiated surfaces had almost zero. On the other hand, our previous study has shown that the monoclinic ratio of the original YSZ surface was about 3%, and the pore-processed surface, which is shown as "unirradiated" in Figure 15, was about the same [29]. In general, the thermal effects during the process such as temperature change cause a tetragonal–to–monoclinic phase transformation of YSZ, degrading its mechanical material properties. YSZ has extremely high strength and toughness among ceramic materials and even zirconia-based ceramic materials due to the stress-induced toughening mechanism and is applied to products that require high strength and toughness such as dental materials, biomaterials, and mechanical parts. If the mechanical properties of the original YSZ are compromised due to a significant increase in the monoclinic phase on the YSZ surface during processing, the strength of the substrate itself will decrease even if silver is embedded in the YSZ surface, and the product life will be shortened due to

damage from cracking. Furthermore, fracture on the surface can easily expose and release the silver embedded in the pores, which causes the loss functionalizing effect of the silver. Hence, an additional surface treatment method that prevents the increase of the monoclinic phase is required. In this study, the formation of silver nanoparticle-embedded pores was achieved by using laser irradiation at very low laser fluence without causing the significant phase transformation of the YSZ substrate itself, i.e., without causing any thermal damage to the bulk.

3.6. Mechanism of Silver Implantation

Based on the aforementioned results, a nanoparticle-embedded process in the nanopore during laser irradiation was summarized. The mechanism of change in surface morphology is schematically shown in Figure 16.
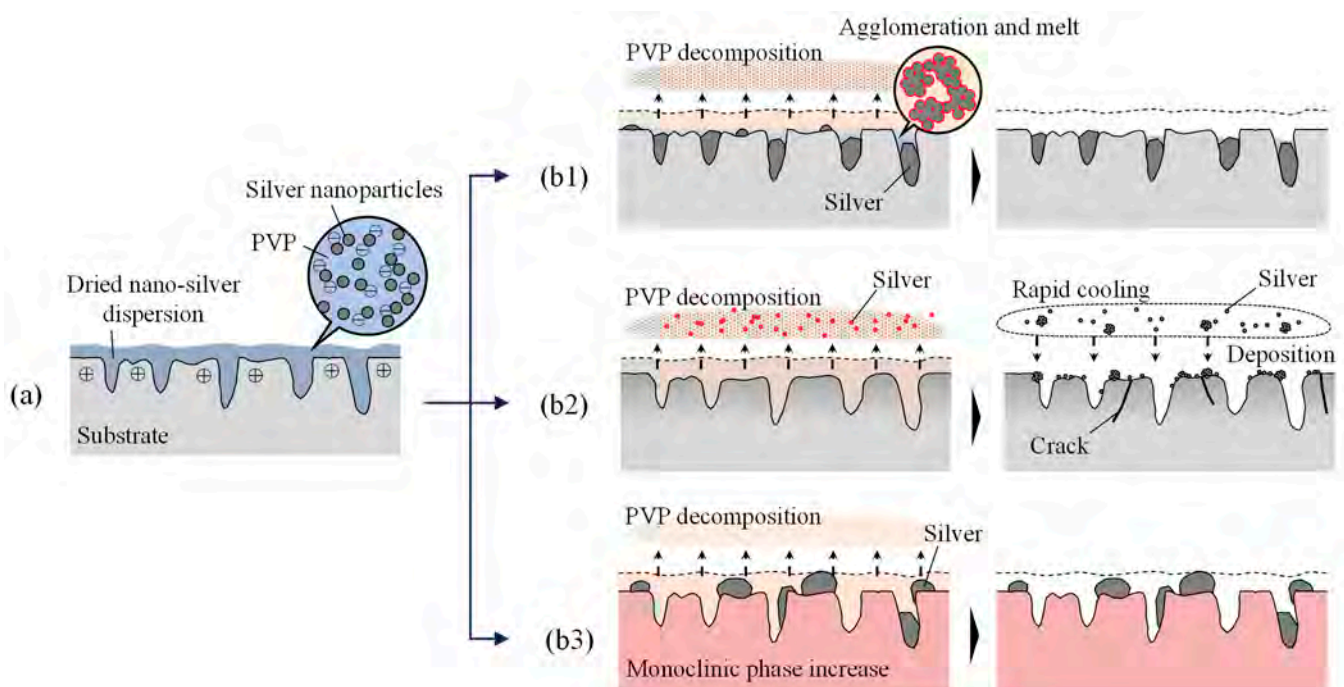

Figure 16. Difference in material behavior on the surface: (**a**) dropping nano-silver dispersion on YSZ surface after nanopore generation, (**b1**) irradiation by femtosecond pulsed laser, (**b2**) irradiation by nanosecond pulsed laser, (**b3**) heating in an electric furnace.

After pore fabrication, the YSZ surface is slightly positively charged. In addition, the surface becomes hydrophilic as reported in our previous study [29]. Therefore, when a nano-silver dispersion liquid is dropped, the liquid spreads widely on the surface, and the negatively charged silver nanoparticles are adsorbed by Coulomb force (Figure 16a). Since the samples are placed in a vacuum desiccator, it is assumed that the degassing action will allow the dispersion to penetrate the pores. After the water is gone and dried, the dispersant PVP remains with a large amount of silver nanoparticles (Figure 3). In this study, when the laser irradiation was performed at a fluence extremely smaller than the ablation threshold of the YSZ, only the surface PVP film was removed without machining the YSZ surface.

PVP is one of the most commonly used materials for dispersion of metal nanoparticles. Removal by combustion has been reported in many cases. For example, Taguchi et al. [40] proposed a method to remove PVP from Pt nanocolloids by multiple washing with solvent and combustion. In the case of this study, the removal of PVP was realized by the role of laser irradiation as one of the methods for combustion.

Since metal nanoparticles enhance the combustion of PVP, the glass transition temperature of PVP is about 180 °C, and the decomposition temperature is about 380 °C [41]. The

melting point of bulk silver is about 960 °C [42], but the melting point of silver nanoparticles may have changed due to nanoparticulation. Feng et al. [43] reported that the melting point of single nanoparticles or nanoparticle clusters significantly decreased compared to the bulk material due to the size effect. Therefore, it is assumed that the melting point of silver nanoparticles used in this study is also smaller than that of bulk silver.

In laser processing of polymer materials, ablation by laser pulses breaks down the polymer into gases and removes it from the surface [44]. When metal nanoparticles are included, the interfacial interaction between the particles and the polymer matrix in contact with them promotes the heating and melting of the polymer, which changes the ablation properties [45,46]. Therefore, it is considered that the polymer decomposition proceeds through a complex combination of photochemical and thermal reactions acting simultaneously.

From the above, the phenomena on the sample surface during laser irradiation are considered as follows. When irradiated by laser under appropriate conditions, silver nanoparticles aggregate in PVP, which reaches the glass transition point, and melt to form large clumps. Then, PVP decomposes and disperses into the atmosphere, leaving mainly silver on the YSZ. Here, at any pulse width and laser fluence, the surface morphology did not change when the scanning speed was greater than a certain value. This indicates that PVP cannot be decomposed by single pulse irradiation but is gradually decomposed by repeated irradiation at the same location.

When an ultrashort pulsed laser is used (Figure 16(b1)), the silver clumps remaining on the YSZ surface are gradually ablated and removed due to multiple pulse irradiation. However, small clumps deep within the elongated nanopores surrounded by zirconia, which has a very low thermal conductivity compared to silver, are less affected by the laser beam and remain within the pore as clumps.

When irradiated with a nanosecond pulsed laser with a large pulse width (Figure 16(b2)), the entire dried dispersion film is heated, and its temperature increases. From the experimental results, surfaces irradiated with nanoseconds were melted as shown in Figure 8. Considering that the melting point of zirconia is about 2700 °C, both PVP and silver nanoparticles (boiling point of bulk silver is about 2160 °C [47]) become vaporized and leave the YSZ surface. Some vaporized silver cools down rapidly, and agglomerates in the air become tiny nanoparticles, which are again deposited on the YSZ surface.

When heated in an electric furnace at 450 °C (Figure 16(b3)), a little higher than the decomposition temperature of PVP, large clumps of silver nanoparticles adhered to the YSZ surface. However, most of these clumps remained above the pores and did not penetrate the pores. This heating temperature was suitable for the decomposition and removal of PVP, but not for melting the silver and allowing it to flow onto the surface and into the pore for implantation. Moreover, the heat applied to the sample at this temperature for a considerably longer time than the laser irradiation caused a phase transformation of the YSZ, resulting in a large increase in monoclinic phases. Thus, the ultrashort laser pulse is considered to be suitable for removing only the surface layer of PVP and melting the silver to be embedded in the pore.

Consider the difference in surface morphology depending on the laser irradiation parameters. When the scanning speed is too large, the number of pulses is insufficient and the PVP remains undecomposed. On the other hand, the smaller the scanning speed, the more the laser is repeatedly irradiated to the surface with nanopores once the surface-dried film is removed and the surface is bare. Then, the material remaining in the pore is easily removed by direct interaction with the laser beam. Since the threshold of the number of pulses that can decompose PVP changes with laser fluence, the suitable scanning speed also changes accordingly. Furthermore, at very low laser fluence, the increase in overlap rate is thought to promote the formation of LIPSS. At high fluence, the YSZ itself is processed, where the surface area is increased by nanopore formation and the ablation threshold becomes lower than the original YSZ, as shown in Figure 5.

In addition to laser parameter control during PVP removal, there are other factors to consider to obtain a more uniform silver-embedded surface. First, by applying the nano-silver dispersion liquid evenly to YSZ to maintain a constant dried film thickness, it is thought that the dried film will be removed evenly during laser irradiation, and the adhesion of residual PVP debris can be suppressed. Furthermore, it is necessary to process the nanopores with high density and uniformity. In this study, laser irradiation was performed using a circular Gaussian beam, which creates gaps between pulses. Therefore, it is considered effective to use, for example, a square laser beam with a flat-top energy distribution, and a line beam laser. In this method, a commercially available nano-silver dispersion was used. According to the above discussion, the dispersant PVP is thought to be suitable for embedding silver nanoparticles in nanopores because it is water-soluble, easily wets and spreads silver on the YSZ surface, and decomposes at a relatively low temperature. Although silver nanoparticles of a few nanometers in diameter were used, methods for generating particles of various sizes have been reported in recent years [48], and changes in embedding phenomena with particle size also require investigation.

Based on the above results, the advantage of the silver embedding method proposed in this study is summarized. Table 3 shows some of the methods for loading materials on the material surface. There are several methods for loading silver nanoparticles, including depositing silver using a chemical solution such as silver nitrate solution (Table 3 (a)), irradiating a silver substrate with a laser and trapping the scattered nanoparticles in suspension (Table 3 (b)), and having the nanoparticles deposited on the surface in a nano-silver solution (Table 3 (c)). In these methods, the nanoparticles adhere to the entire treated surface. In some cases, the particles do not penetrate the interior of the structure and are not fixed. On the other hand, the method proposed in this study uses silver nanoparticles in a commercially available nano-silver dispersion, and silver can be placed in targeted areas by controlling the processing position of nanopores. The re-irradiation of the laser beam also separates the PVP from the silver and removes excess material from the surface, so the substrate surface is not covered with the embedded material. The silver nanoparticles penetrate deep into the pores and form large clumps that can be anchored in the pores. The amount of embedded silver can be controlled by the laser parameters. No special equipment or chemicals are required, and thermal damage to the substrate during the process can be suppressed. The effectiveness of laser patterning nanoarrays for material fixation on fused silica surfaces was reported (Table 3 (d)). However, such a nanoarray fabrication technique for YSZ has not yet been reported. In our study, a novel technique to form a large number of nanopores on the YSZ surface at once using a femtosecond pulsed laser was used to achieve the loading onto the surface nanostructures.

Table 3. Material loading methods.

	Substrate Material	Substrate Structure	Embedding Material	Embedding Method	Ref.
(a)	Cellulose nanofiber (CNF)	Nanofiber	Ag nanoparticle	High-pressure wet-type jet mill	[8]
(b)	Graphene oxide (GO)	Nanosheet	Ag nanoparticle	Laser ablation in GO suspension	[7]
(c)	Titanium	Polished flat surface	Ag nanoparticle	Deposition in silver nanoparticle solution	[49]
(d)	Fused silica	Nanopore arrays	Peptide	Adsorption	[10]
(e)	Yttria-stabilized zirconia (YSZ)	Nanopores	Ag nanoparticle	Laser irradiation	This study

4. Conclusions

Femtosecond pulsed laser irradiation was performed to embed silver nanoparticles in nanopores on YSZ, and its fundamental characteristics were investigated. The conclusions are summarized as follows.

(1)　Silver nanoparticles were successfully embedded in nanopores generated by irradiating a YSZ substrate with a femtosecond pulsed laser, by dropping a commercially available nano-silver dispersion into the pores and re-irradiating the laser.

(2)　By irradiating at the fluence in a limited range much lower than the ablation threshold, the polyvinylpyrrolidone (PVP) polymer dispersant remaining on the outer surface

of the nanopores was selectively decomposed and removed. On the other hand, increasing the fluence at low scanning speeds caused delamination of the YSZ substrate surface and the formation of laser-induced periodic surface structures. Laser fluence and scanning speed interacted to embed silver in the pores while maintaining the grain shape of the substrate surface. The best conditions in this study were laser fluence of 0.6 J/cm^2 and scanning speed of 200 mm/s, at which the silver implantation rate reached about 60%.

(3) When the pulse width was increased, the substrate surface melted and a crack occurred due to the thermal effect. At the same time, not only the PVP but also silver was removed from both the surface and inside the pores, indicating that ultrashort pulses are suitable for maintaining the substrate surface morphology and silver loading.

(4) The silver nanoparticles melted and agglomerated, forming large agglomerates inside the nanopores by laser irradiation while separated from the dispersant PVP. The silver was embedded to the bottom of the elongated pore, reaching a depth of approximately 600 nm from the surface.

(5) The thermally induced tetragonal–to–monoclinic phase transformation was suppressed on the YSZ surface after embedding silver nanoparticles in the nanopore by using low laser fluence under the ablation threshold, indicating no thermal damage to the bulk.

This study demonstrated the new approach to the functionalization of YSZ surfaces by implanting different materials in nanopores by the femtosecond pulsed laser process without causing severe thermal damage to the bulk. This technique enabled the local embedding of metal nanoparticles without causing significant thermal damage to the bulk. The method can be expected to be a cost-effective system, as it can be completed using only a low-power femtosecond pulsed laser system and requires a small amount of commercially available silver nanoparticles. In addition to the surface features of zirconia, such as biocompatibility, silver-loaded YSZ substrates are expected to have a synergistic effect due to the sustained antimicrobial effect of silver fixed in the surface nanopores. These findings not only deepen the scientific understanding of the ablation properties of the different materials on the substrate, but also provide the potential to expand new applications for zirconia by adding value through surface functionality such as antibacterial properties, biocompatibility, and nanomedicine delivery. To further develop this study, it is necessary to evaluate the long-term stability of silver embedded in nanopores and its behavior under other environmental conditions and verify its functionality in the future. In addition, optimization of unexplored laser parameters is required to improve the silver embedding rate.

References

1. Garvie, R.C.; Hannink, R.H.; Pascoe, R.T. Ceramic Steel? *Nature* **1975**, *258*, 703–704. [CrossRef]
2. Chen, F.; Zhang, D.; Yang, Q.; Yong, J.; Du, G.; Si, J.; Yun, F.; Hou, X. Bioinspired Wetting Surface via Laser Microfabrication. *ACS Appl. Mater. Interfaces* **2013**, *5*, 6777–6792. [CrossRef]
3. Yao, L.; He, J. Recent Progress in Antireflection and Self-Cleaning Technology—From Surface Engineering to Functional Surfaces. *Prog. Mater. Sci.* **2014**, *61*, 94–143. [CrossRef]
4. Hou, P.J.; Ou, K.L.; Wang, C.C.; Huang, C.F.; Ruslin, M.; Sugiatno, E.; Yang, T.S.; Chou, H.H. Hybrid Micro/Nanostructural Surface Offering Improved Stress Distribution and Enhanced Osseointegration Properties of the Biomedical Titanium Implant. *J. Mech. Behav. Biomed. Mater.* **2018**, *79*, 173–180. [CrossRef] [PubMed]
5. Schünemann, F.H.; Galárraga-Vinueza, M.E.; Magini, R.; Fredel, M.; Silva, F.; Souza, J.C.M.; Zhang, Y.; Henriques, B. Zirconia Surface Modifications for Implant Dentistry. *Mater. Sci. Eng. C* **2019**, *98*, 1294–1305. [CrossRef] [PubMed]
6. Ji, M.; Xu, J.; Chen, M.; El Mansori, M. Enhanced Hydrophilicity and Tribological Behavior of Dental Zirconia Ceramics Based on Picosecond Laser Surface Texturing. *Ceram. Int.* **2020**, *46*, 7161–7169. [CrossRef]
7. Nancy, P.; Jose, J.; Joy, N.; Valluvadasan, S.; Philip, R.; Antoine, R.; Thomas, S.; Kalarikkal, N. Fabrication of Silver-Decorated Graphene Oxide Nanohybrids via Pulsed Laser Ablation with Excellent Antimicrobial and Optical Limiting Performance. *Nanomaterials* **2021**, *11*, 880. [CrossRef] [PubMed]
8. Furutani, M.; Fujii, E.; Ogura, K. Immobilization of Silver Nanoparticles on the Surface of Cellulose Nanofibers Using High-Pressure Wet-Type Jet Mill. *J. Soc. Mater. Sci.* **2021**, *70*, 400–405. [CrossRef]
9. Zheng, K.; Setyawati, M.I.; Leong, D.T.; Xie, J. Antimicrobial Silver Nanomaterials. *Coord. Chem. Rev.* **2018**, *357*, 1–17. [CrossRef]
10. Zachman, A.L.; Hofmeister, L.H.; Costa, L.; Boire, T.C.; Hwang, Y.S.; Hofmeister, W.H.; Sung, H.J. Femtosecond Laser-Patterned Nanopore Arrays for Surface-Mediated Peptide Treatment. *Nanomed. Nanotechnol. Biol. Med.* **2014**, *10*, 11–14. [CrossRef]
11. Losic, D.; Simovic, S. Self-Ordered Nanopore and Nanotube Platforms for Drug Delivery Applications. *Expert. Opin. Drug Deliv.* **2009**, *6*, 1363–1381. [CrossRef] [PubMed]
12. Smielak, B.; Klimek, L. Effect of Hydrofluoric Acid Concentration and Etching Duration on Select Surface Roughness Parameters for Zirconia. *J. Prosthet. Dent.* **2015**, *113*, 596–602. [CrossRef] [PubMed]
13. Sriamporn, T.; Thamrongananskul, N.; Busabok, C.; Poolthong, S.; Uo, M.; Tagami, J. Dental Zirconia Can Be Etched by Hydrofluoric Acid. *Dent. Mater. J.* **2014**, *33*, 79–85. [CrossRef]
14. Scott, H.G. Phase Relationships in the Zirconia-Yttria System. *J. Mater. Sci.* **1975**, *10*, 1527–1535. [CrossRef]
15. Gupta, T.K.; Lange, F.F.; Bechtold, J.H. Effect of Stress-Induced Phase Transformation on the Properties of Polycrystalline Zirconia Containing Metastable Tetragonal Phase. *J. Mater. Sci.* **1978**, *13*, 1464–1470. [CrossRef]
16. Kosmač, T.; Oblak, Č.; Marion, L. The Effects of Dental Grinding and Sandblasting on Ageing and Fatigue Behavior of Dental Zirconia (Y-TZP) Ceramics. *J. Eur. Ceram. Soc.* **2008**, *28*, 1085–1090. [CrossRef]
17. Grigore, A.; Spallek, S.; Petschelt, A.; Butz, B.; Spiecker, E.; Lohbauer, U. Microstructure of Veneered Zirconia after Surface Treatments: A TEM Study. *Dent. Mater.* **2013**, *29*, 1098–1107. [CrossRef]
18. Bakkar, S.; Pantawane, M.V.; Gu, J.J.; Ghoshal, A.; Walock, M.; Murugan, M.; Young, M.L.; Dahotre, N.; Berman, D.; Aouadi, S.M. Laser Surface Modification of Porous Yttria Stabilized Zirconia against CMAS Degradation. *Ceram. Int.* **2020**, *46*, 6038–6045. [CrossRef]
19. Yang, L.; Wei, J.; Ma, Z.; Song, P.; Ma, J.; Zhao, Y.; Huang, Z.; Zhang, M.; Yang, F.; Wang, X. The Fabrication of Micro/Nano Structures by Laser Machining. *Nanomaterials* **2019**, *9*, 1789. [CrossRef]
20. White, Y.V.; Li, X.; Sikorski, Z.; Davis, L.M.; Hofmeister, W. Single-Pulse Ultrafast-Laser Machining of High Aspect Nano-Holes at the Surface of SiO2. *Opt. Express* **2008**, *16*, 14411–14420. [CrossRef]
21. Lu, Y.; Kai, L.; Yang, Q.; Du, G.; Hou, X.; Chen, F. Laser Fabrication of Nanoholes on Silica through Surface Window Assisted Nano-Drilling (Swan). *Nanomaterials* **2021**, *11*, 3340. [CrossRef]
22. Rajput, D.; Crowder, S.W.; Hofmeister, L.; Costa, L.; Sung, H.J.; Hofmeister, W. Cell Interaction Study Method Using Novel 3D Silica Nanoneedle Gradient Arrays. *Colloids Surf. B Biointerfaces* **2013**, *102*, 111–116. [CrossRef] [PubMed]
23. Zamfirescu, M.; Ulmeanu, M.; Jipa, F.; Anghel, I.; Simion, S.; Dabu, R.; Ionita, I. Laser Processing and Characterization with Femtosecond Laser Pulses. *Rom. Rep. Phys.* **2010**, *62*, 594–609.
24. Kobayashi, T.; Yan, J. Generating Nanodot Structures on Stainless-Steel Surfaces by Cross Scanning of a Picosecond Pulsed Laser. *Nanomanufacturing Metrol.* **2020**, *3*, 105–111. [CrossRef]
25. Sakaue, K.; Motoyama, H.; Hayashi, R.; Iwasaki, A.; Mimura, H.; Yamanouchi, K.; Shibuya, T.; Ishino, M.; Dinh, T.-H.; Ogawa, H.; et al. Surface Processing of PMMA and Metal Nano-Particle Resist by Sub-Micrometer Focusing of Coherent Extreme Ultraviolet High-Order Harmonics Pulses. *Opt. Lett.* **2020**, *45*, 2926. [CrossRef]
26. Yamamuro, Y.; Shimoyama, T.; Yamashita, I.; Yan, J. Multiscale Surface Patterning of Zirconia by Picosecond Pulsed Laser Irradiation. *J. Micro Nano-Manuf.* **2020**, *8*, 8–13. [CrossRef]
27. Karim, W.; Millon, E.; Vulliet, J.; Tabbal, M.; Thomann, A.; Semmar, N. Applied Surface Science Nano-Squares and Regular LIPSS on YSZ Coating by Picosecond UV Laser Beam: Thin Film Mediated and Direct Texturing. *Appl. Surf. Sci. J.* **2023**, *623*, 157110. [CrossRef]

28. Kakehata, M.; Yashiro, H.; Oyane, A.; Ito, A.; Torizuka, K. Pulsewidth Dependence of Laser-Induced Periodic Surface Structure Formed on Yttria-Stabilized Zirconia Polycrystal. In Proceedings of the Frontiers in Ultrafast Optics: Biomedical, Scientific, and Industrial Applications XVI, San Francisco, CA, USA, 9 March 2016; Heisterkamp, A., Herman, P.R., Meunier, M., Nolte, S., Eds.; SPIE: Bellingham, WA, USA, 2016; Volume 9740, p. 97401G.

29. Yamamuro, Y.; Shimoyama, T.; Yan, J. Generation of Nanopore Structures in Yttria-Stabilized Zirconia by Femtosecond Pulsed Laser Irradiation. *J. Mater. Res. Technol.* **2023**, *23*, 1155–1176. [CrossRef]

30. Mijnendonckx, K.; Leys, N.; Mahillon, J.; Silver, S.; Van Houdt, R. Antimicrobial Silver: Uses, Toxicity and Potential for Resistance. *Biometals* **2013**, *26*, 609–621. [CrossRef]

31. Luo, X.; Yang, L.; Cui, Y. Microneedles: Materials, Fabrication, and Biomedical Applications. *Biomed. Microdevices* **2023**, *25*, 20. [CrossRef]

32. Turon-Vinas, M.; Anglada, M. Strength and Fracture Toughness of Zirconia Dental Ceramics. *Dent. Mater.* **2018**, *34*, 365–375. [CrossRef]

33. Bonse, J.; Hohm, S.; Kirner, S.V.; Rosenfeld, A.; Kruger, J. Laser-Induced Periodic Surface Structures-A Scientific Evergreen. *IEEE J. Sel. Top. Quantum Electron.* **2017**, *23*, 109–123. [CrossRef]

34. Bonse, J.; Kirner, S.V.; Höhm, S.; Epperlein, N.; Spaltmann, D.; Rosenfeld, A.; Krüger, J. Applications of Laser-Induced Periodic Surface Structures (LIPSS). In Proceedings of the Laser-based Micro- and Nanoprocessing XI, San Francisco, CA, USA, 17 February 2017; Klotzbach, U., Washio, K., Kling, R., Eds.; SPIE: Bellingham, WA, USA, 2017; Volume 10092, pp. 1–9.

35. Bonse, J.; Gräf, S. Ten Open Questions about Laser-Induced Periodic Surface Structures. *Nanomaterials* **2021**, *11*, 3326. [CrossRef]

36. Nakajima, A.; Yan, J. Response of Resin Coating Films Containing Fine Metal Particles to Ultrashort Laser Pulses. *Int. J. Precis. Eng. Manuf.* **2022**, *23*, 385–393. [CrossRef]

37. Li, X.; Zhang, Q.; Zhou, X.; Zhu, D.; Liu, Q. The Influence of Nanosecond Laser Pulse Energy Density for Paint Removal. *Optik* **2018**, *156*, 841–846. [CrossRef]

38. Pezzotti, G.; Porporati, A.A. Raman Spectroscopic Analysis of Phase-Transformation and Stress Patterns in Zirconia Hip Joints. *J. Biomed. Opt.* **2004**, *9*, 372. [CrossRef] [PubMed]

39. Muñoz Tabares, J.A.; Anglada, M.J. Quantitative Analysis of Monoclinic Phase in 3Y-TZP by Raman Spectroscopy. *J. Am. Ceram. Soc.* **2010**, *93*, 1790–1795. [CrossRef]

40. Taguchi, A.; Nagaki, Y.; Yoneyama, Y. Solvent Washing and Calcination for Effective PVP-Cap Removal on Pt Nanoparticles. *Annu. Rep. Hydrog. Isot. Res. Cent. Univ. Toyama* **2014**, *34*, 45–50.

41. Rioux, R.M.; Song, H.; Grass, M.; Habas, S.; Niesz, K.; Hoefelmeyer, J.D.; Yang, P.; Somorjai, G.A. Monodisperse Platinum Nanoparticles of Well-Defined Shape: Synthesis, Characterization, Catalytic Properties and Future Prospects. *Top. Catal.* **2006**, *39*, 167–174. [CrossRef]

42. Preston-Thomas, H. The International Temperature Scale of 1990 (ITS-90). *Metrologia* **1990**, *27*, 3–10. [CrossRef]

43. Feng, D.; Feng, Y.; Yuan, S.; Zhang, X.; Wang, G. Melting Behavior of Ag Nanoparticles and Their Clusters. *Appl. Therm. Eng.* **2017**, *111*, 1457–1463. [CrossRef]

44. Lippert, T.; Hauer, M.; Phipps, C.R.; Wokaun, A. Fundamentals and Applications of Polymers Designed for Laser Ablation. *Appl. Phys. A Mater. Sci. Process.* **2003**, *77*, 259–264. [CrossRef]

45. Zeng, R.; Rong, M.Z.; Zhang, M.Q.; Liang, H.C.; Zeng, H.M. Laser Ablation of Polymer-Based Silver Nanocomposites. *Appl. Surf. Sci.* **2002**, *187*, 239–247. [CrossRef]

46. Zhao, H.C.; Qiao, Y.L.; Zhang, Q.; Du, X.; Zang, Y.; Liu, X.T.; Han, B.Y. Study on the Characteristics and Mechanism of Pulsed Laser Cleaning of Polyacrylate Resin Coating on Aluminum Alloy Substrates. *Appl. Opt.* **2020**, *59*, 7053. [CrossRef] [PubMed]

47. Geiger, F.; Busse, C.A.; Loehrke, R.I. The Vapor Pressure of Indium, Silver, Gallium, Copper, Tin, and Gold Between 0.1 and 3.0 Bar. *Int. J. Thermophys.* **1987**, *8*, 425–435. [CrossRef]

48. Nancy, P.; James, J.; Valluvadasan, S.; Kumar, R.A.V.; Kalarikkal, N. Laser–Plasma Driven Green Synthesis of Size Controlled Silver Nanoparticles in Ambient Liquid. *Nano-Struct. Nano-Objects* **2018**, *16*, 337–346. [CrossRef]

49. Juan, L.; Zhimin, Z.; Anchun, M.; Lei, L.; Jingchao, Z. Deposition of Silver Nanoparticles on Titanium Surface for Antibacterial Effect. *Int. J. Nanomed.* **2010**, *5*, 261–267. [CrossRef]